

Improved model for the dissociative sequential double ionization of nitrogen molecules by an intense few-cycle infrared laser pulse

Yan-Wen Jia,¹ C. H. Yuen^{2,3,*}, Wen-Quan Jing¹, Zhong-Yao Zhou,¹ C. D. Lin^{3,†} and Song-Feng Zhao^{1,‡}
¹College of Physics and Electronic Engineering, Northwest Normal University, Key Laboratory of Atomic and Molecular Physics and Functional Materials of Gansu Province, Lanzhou 730070, Peoples Republic of China
²Department of Physics, Kennesaw State University, Marietta, Georgia 30060, USA
³J. R. Macdonald Laboratory, Department of Physics, Kansas State University, Manhattan, Kansas 66506, USA

 (Received 10 July 2024; accepted 13 August 2024; published 26 August 2024)

A density matrix approach was recently developed by Yuen and Lin to study the dissociative sequential double ionization (SDI) of N₂ molecules induced by an intense few-cycle infrared laser pulse [Phys. Rev. A **106**, 023120 (2022)]. Despite the positions and relative ratios of peaks in the simulated kinetic energy release (KER) spectrum agreeing very well with experiments, the experimental KER spectrum is considerably broader than that obtained from the simulation where both laser couplings between N₂²⁺ states and the nuclear vibration distribution of neutral N₂ molecules were neglected. Here, we revisit to simulate the experiment by Voss *et al.* [J. Phys. B: At. Mol. Opt. Phys. **37**, 4239 (2004)] and Wu *et al.* [J. Phys. Chem. A **114**, 6751 (2010)] and find that the agreement between the simulated KER spectra and the experiments is improved significantly by considering the laser couplings between N₂²⁺ states and nuclear vibration distribution of neutral N₂ molecules. This work provides further insights into the SDI dynamics and the influences of nuclear motion on the SDI of molecules.

DOI: [10.1103/PhysRevA.110.023112](https://doi.org/10.1103/PhysRevA.110.023112)

I. INTRODUCTION

Since the sequential double ionization (SDI) of diatomic molecules N₂ and O₂ was reported experimentally using a time-of-flight mass spectrometer in 1998 [1], there has been extensive research on the SDI of both diatomic molecules [2–6] and polyatomic molecules [7–14] in intense infrared (IR) laser fields. These investigations have primarily utilized coincidence measurement techniques, such as the cold-target recoil-ion reaction momentum spectroscopy [15,16] and velocity map imaging [17], producing multidimensional data for the momenta of ionic fragments and ionized electrons. Theoretically, several advanced *ab initio* methods have been employed to model the SDI of molecules, including the time-dependent Schrödinger equation [18], real-time time-dependent density functional theory [19], time-dependent configuration interaction with singly excited configurations and a complex absorbing potential [20,21], and Monte Carlo wave packet [22]. However, these methods are computationally expensive for simulating the SDI of randomly oriented molecules. Recently, Yuen and Lin developed a density matrix approach for SDI of molecules driven by an intense few-cycle IR pulse that can efficiently simulate observables under experimental conditions [23–26]. This method, called the DM-SDI, has also been applied to investigate the vibronic coherence in attosecond charge migration [27,28].

In previous work [23], we simulated the experimental data for N₂ SDI from Voss *et al.* [3] and Wu *et al.* [4] using

the DM-SDI model assuming that the nuclei are frozen at the equilibrium geometry of the neutral and that the ionized electrons and laser couplings between N₂²⁺ states are unimportant. Although the positions and relative ratios of peaks in the simulated kinetic energy release (KER) spectrum agree very well with the experimental data, the experimental KER spectrum is much broader than those from the DM-SDI model. By assuming SDI occurs vertically, one can broaden the KER spectrum by applying the DM-SDI model at different initial internuclear distances. In this article, we improve the DM-SDI model by including the laser couplings between the N₂²⁺ states and the vibrational motion of the ground state X¹Σ_g⁺ of neutral N₂. We find that these laser couplings play a crucial role in N₂ SDI, and the revised DM-SDI model can reproduce more features in the experimental KER spectra [3,4], highlighting the importance of vibrational motion in the neutral ground state.

This article is arranged as follows: In the next section, we briefly review the DM-SDI model. In Sec. III, we investigate the effects of laser couplings between doubly charged states and nuclear vibrational motion of the neutral N₂ on the KER spectra. Finally, we summarize the results and provide an outlook for future research in Sec. IV.

II. THEORETICAL METHODS

In the DM-SDI model, the ionized electrons are neglected and the residual ion and dication become open systems. Here, we follow the model in Ref. [23] and neglect the coherence build-up from tunnel ionization [24]. The equations for the time evolution of the density matrices of different charges are

$$\frac{d\rho^{(q)}}{dt} = -\frac{i}{\hbar}[H^{(q)}, \rho^{(q)}] + \Gamma^{(q)}(t), \quad (1)$$

*Contact author: cyuen2@kennesaw.edu

†Contact author: cdlin@phys.ksu.edu

‡Contact author: zhaosf@nwnu.edu.cn

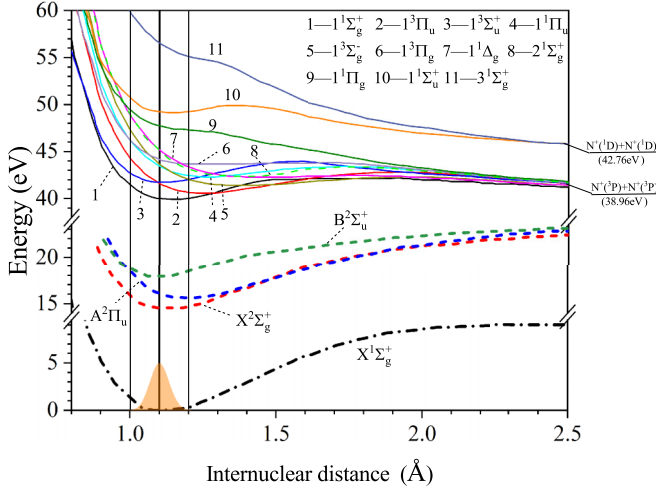


FIG. 1. The potential energy curves of N_2 , N_2^+ and N_2^{2+} , extracted from Ref. [29]. States 1–11 correspond to the N_2^{2+} states described in Table I. The orange shaded area represents the initial nuclear wave packet.

with ionization matrices $\Gamma^{(q)}$ as

$$\Gamma^{(0)}(t) = - \sum_i \rho^{(0)}(t) W_i^{(0)}(t), \quad (2)$$

$$\Gamma_{ij}^{(1)}(t) = \delta_{ij} \left[\rho^{(0)}(t) W_i^{(0)}(t) - \sum_n \rho_{ii}^{(1)}(t) W_{n \leftarrow i}^{(1)}(t) \right], \quad (3)$$

$$\Gamma_{mn}^{(2)}(t) = \delta_{mn} \sum_i \rho_{ii}^{(1)}(t) W_{n \leftarrow i}^{(1)}(t). \quad (4)$$

In the above, the density matrix $\rho^{(q)}$ represents the different charged states, with $q = 0, 1, 2$ corresponding to the neutral, ionic, and doubly charged states. The ionization rate from the neutral ground state to the i th ionic state is denoted as $W_i^{(0)}$, while $W_{n \leftarrow i}^{(1)}$ represents the ionization rate from the i th ionic state to the n th doubly charged state. All the ionization rates were calculated according to the molecular Ammosov-Delone-Krainov (MO-ADK) theory [30,31]. The diagonal

elements of the Hamiltonian $H^{(q)}$ are $H_{mm}^{(q)} = I_p^{(q)}$, which are the vertical ionization potentials. The off-diagonal elements are defined as $H_{mn}^{(q)} = -\vec{d}_{mn}^{(q)} \cdot \vec{E}$, with \vec{d} denoting the transition dipole moment and \vec{E} representing the laser field. Throughout this article, the laser field takes the form

$$\vec{E}(t) = E_0 e^{-2 \ln 2 (t^2/\tau^2)} \cos \omega t \hat{e}, \quad (5)$$

where τ denotes the full width at half maximum (FWHM), ω represents the central frequency, and \hat{e} is the polarization vector on the xz plane. The molecular axis of N_2 is aligned with the z axis, while the laser propagates along the y axis. Equation (1) is solved using the fixed-step fourth-order Runge-Kutta method with initial conditions $\rho^{(0)}(t_0) = 1$ and $\rho^{(1)}(t_0) = \rho^{(2)}(t_0) = 0$. The probability of forming the n th doubly charged state from SDI is given by $P_n = \rho_{nn}^{(2)}(t \rightarrow \infty)$.

To understand the SDI process of N_2 , the potential energy curves (PECs) of N_2 , N_2^+ , and N_2^{2+} states [29] are depicted in Fig. 1. The vertical black line at $R = 1.10 \text{ \AA}$ represents the equilibrium internuclear distance. The vibrational range of the neutral molecule covers from $R = 1.00$ to 1.20 \AA , and the orange shaded area denotes the nuclear wave packet of the ground state of the neutral N_2 molecule. The states 1–11 in Fig. 1 are the doubly charged states, and their I_p at different internuclear distances are listed in Table I. The SDI process of N_2 is described as follows: First, the neutral N_2 initially undergoes tunnel ionization, resulting in the formation of $X^2\Sigma_g^+$, $A^2\Pi_u$, and $B^2\Sigma_u^+$ states. Subsequently, these N_2^+ states are coupled by the laser field and further undergo tunnel ionization to yield various N_2^{2+} states, which are also coupled by the laser field. Finally, dissociation occurs for all N_2^{2+} states except for the metastable 1–4 states. These metastable states could potentially undergo transitions to the dissociative states through laser couplings, which were not considered in our early work [23].

In the MO-ADK theory [30], the ionization rate depends on structure parameters which can be extracted from the asymptotic wave function of the molecular orbital from which the electron is removed. In our previous works [34,35], we

TABLE I. Indices 1–11 represent the N_2^{2+} states with two valence holes. The vertical ionization energies at different internuclear distances are obtained from Pandey *et al.* [32]. Dissociation limits of the N_2^{2+} states are adopted from Iwayama *et al.* [33]. The limit of the $1^1\Sigma_u^+$ and $3^1\Sigma_g^+$ states are identified from the PECs from Ref. [29]. Metastable states are denoted as m.s. in Table I.

Index	State	Config.	Limit	I_p (eV)				
				$R = 1.00 \text{ \AA}$	1.05 \AA	1.10 \AA	1.15 \AA	1.20 \AA
1	$1^1\Sigma_g^+$	$3\sigma_g^{-2}$	m.s.	43.72	42.86	42.49	42.46	42.64
2	$1^3\Pi_u$	$1\pi_u^{-1}3\sigma_g^{-1}$	m.s.	45.97	44.41	43.42	42.86	42.60
3	$1^3\Sigma_u^+$	$2\sigma_u^{-1}3\sigma_g^{-1}$	m.s.	44.70	44.08	43.94	44.12	44.48
4	$1^1\Pi_u$	$1\pi_u^{-1}3\sigma_g^{-1}$	m.s.	47.54	45.94	44.93	44.34	44.05
5	$1^3\Sigma_g^-$	$1\pi_u^{-2}$	$N^+(^3P)+N^+(^3P)$	49.00	46.93	45.50	44.54	43.92
6	$1^3\Pi_g$	$2\sigma_u^{-1}1\pi_u^{-1}$	$N^+(^3P)+N^+(^3P)$	48.17	46.97	46.29	45.99	45.91
7	$1^1\Delta_g$	$1\pi_u^{-2}$	$N^+(^3P)+N^+(^3P)$	50.16	48.02	46.52	45.50	44.81
8	$2^1\Sigma_g^+$	$1\pi_u^{-2}$	$N^+(^3P)+N^+(^3P)$	49.54	47.87	46.54	45.51	45.15
9	$1^1\Pi_g$	$2\sigma_u^{-1}1\pi_u^{-1}$	$N^+(^3P)+N^+(^3P)$	50.69	49.58	48.99	48.76	48.71
10	$1^1\Sigma_u^+$	$2\sigma_u^{-1}3\sigma_g^{-1}$	m.s./ $N^+(^1D)+N^+(^1D)$	51.67	50.81	50.42	50.37	50.52
11	$3^1\Sigma_g^+$	$2\sigma_u^{-2}$	$N^+(^1D)+N^+(^1D)$	59.81	57.80	56.55	55.55	55.09

TABLE II. The C_l coefficient of $3\sigma_g$, $1\pi_u$, and $2\sigma_u$ orbitals of N_2 at different internuclear distances. For σ orbitals, $m = 0$, and for the π orbital, $m = 1$. The present calculated binding energies with the modified Leeuwen-Baerends (LB α) model (see Ref. [35] and the references therein) and those obtained from the multireference configuration interaction (MRCI) method following the complete active space self-consistent field (CASCF) method (i.e., C+M) [29] are also listed.

Orbitals	R (Å)	LB α	I_p (eV)	C_l			α
				C+M	C_{0m}	C_{2m}	
$3\sigma_g$	1.00	15.92	15.69	3.11	1.30	0.09	1.15
	1.05	15.57	15.53	3.25	1.58	0.13	1.08
	1.10	15.60	15.49	2.99	1.48	0.12	1.13
	1.15	15.03	15.23	2.56	1.26	0.11	1.14
	1.20	15.27	15.03	2.89	1.57	0.15	1.11
					C_{1m}	C_{3m}	C_{5m}
$1\pi_u$	1.00	18.15	17.54	2.34	0.29	0.01	1.15
	1.05	17.19	17.33	2.41	0.40	0.03	1.08
	1.10	16.98	16.42	2.15	0.37	0.00	1.13
	1.15	16.17	15.83	1.80	0.30	0.02	1.14
	1.20	15.94	15.69	1.97	0.37	0.03	1.11
					C_{1m}	C_{3m}	C_{5m}
$2\sigma_u$	1.00	17.49	18.40	3.67	0.42	0.02	1.15
	1.05	18.13	18.41	4.53	0.57	0.04	1.08
	1.10	18.14	18.72	4.22	0.55	0.04	1.13
	1.15	17.55	18.67	3.56	0.49	0.00	1.14
	1.20	18.86	18.73	4.71	0.71	0.05	1.11
					C_{1m}	C_{3m}	C_{5m}

constructed numerically a one-electron model potential for linear molecules using density functional theory and obtained molecular wave functions with the correct asymptotic behavior by solving the time-independent Schrödinger equation of molecules with the B -spline basis functions. Then, accurate structure parameters can be determined by a fitting procedure in the asymptotic region. For the first ionization, structure parameters for highest occupied molecular orbital (HOMO), HOMO-1, and HOMO-2 of N_2 at different internuclear distances are calculated using the method of Zhao *et al.* [34,35] and are tabulated in Table II. For the second ionization, we assume that the structure parameters of HOMO, HOMO-1, and HOMO-2 of N_2^+ are the same as those of N_2 .

Another input to the model are the transition dipole moments between N_2^+ and between N_2^{2+} states. Transition dipole moments between N_2^+ states at different internuclear distances are taken from Refs. [36,37] and are listed in Table III of this article. The transition dipole moments between N_2^{2+} states listed in Table IV are calculated using the state-averaged complete active space self-consistent field method with the rotated multistate complete active space second-order perturbation theory in OPENMOLCAS [38]. The large atomic natural orbital basis set was used. Eight electrons were put into an active space of 11 orbitals. For the singlet and triplet N_2^{2+} states, 9 and 6 states were included, respectively.

TABLE III. Transition dipole moments (a.u.) for $X^2\Sigma_g^+ - A^2\Pi_u$ [36] and $X^2\Sigma_g^+ - B^2\Sigma_u^+$ [37].

R (units of a_0)	State 1 \rightarrow 2	
	$X^2\Sigma_g^+ \rightarrow A^2\Pi_u$	$X^2\Sigma_g^+ \rightarrow B^2\Sigma_u^+$
1.80	0.284 \hat{x}	0.822 \hat{z}
1.90	0.279 \hat{x}	0.795 \hat{z}
2.00	0.271 \hat{x}	0.764 \hat{z}
2.10	0.262 \hat{x}	0.729 \hat{z}
2.20	0.251 \hat{x}	0.689 \hat{z}
2.30	0.239 \hat{x}	0.640 \hat{z}
2.40	0.226 \hat{x}	0.578 \hat{z}

III. RESULTS AND DISCUSS

A. Effect of laser couplings between N_2^{2+} states on the SDI of N_2

By solving Eq. (1), we obtain the probability of forming different N_2^{2+} states at different alignment angles θ . The molecule is assumed to be randomly aligned. The alignment-averaged probability for the n th N_2^{2+} state at the equilibrium internuclear distance is

$$\bar{P}_n = \frac{1}{2} \int_0^\pi P_n(\theta) \sin \theta d\theta. \quad (6)$$

The signal of KER spectra is obtained by convoluting the alignment-averaged probabilities of N_2^{2+} states,

$$S(E) = \sum_n \frac{\bar{P}_n}{\sqrt{2\pi\sigma^2}} \exp\left[-\frac{(E - E_n)^2}{2\sigma^2}\right], \quad (7)$$

where E_n denotes the KER of state n and σ is energy resolution. The KER values at different internuclear distances are the difference between vertical ionization energies and the dissociation limits.

To investigate the effect of laser couplings between doubly charged states on the KER spectra, Eq. (1) for the doubly charged state is solved with and without the commutator term, respectively. The KER spectra simulated by the improved DM-SDI model for N_2 at its equilibrium internuclear distance are shown in Fig. 2. The solid black (solid red) line represents the results with (without) laser couplings between the N_2^{2+} states. As described in Ref. [23], the first peak of the KER spectra at 6.54 eV primarily comes from state 5, while the second peak at 7.43 eV arises from the overlap of states 6–8 and 10. Additionally, the third peak at 10.03 eV is attributed to state 9. State 11 is less susceptible to ionization due to their higher ionization energies. The enhancement of the KER spectrum is significant when considering the laser couplings between doubly charged states. The first, second, and third peaks of the KER spectrum are 4.5, 2.3, and 2.4 times larger than those without laser couplings between N_2^{2+} states, respectively.

To further understand how the laser couplings between N_2^{2+} states affect the KER spectra, in Fig. 3, we show the populations of states 1–10 with and without the laser couplings at the equilibrium distance ($R = 1.10$ Å) with the laser polarization at 45° from the molecular axis. The population of state 11 is much smaller than those of states 1–10 (not shown). As seen in the top panel of Fig. 3, the populations of metastable

TABLE IV. Transition dipole moments (a.u.) between N_2^{2+} at different internuclear distances calculated in this work using OPENMOLCAS [38]. States 1–11 are the same as Table I. The symbol $d_{m \rightarrow n}$ denotes the electronic transition dipole moment between state m and n .

R (Å)	$d_{m \rightarrow n}$									
	$d_{1 \rightarrow 4}$	$d_{1 \rightarrow 10}$	$d_{2 \rightarrow 5}$	$d_{2 \rightarrow 6}$	$d_{3 \rightarrow 6}$	$d_{4 \rightarrow 7}$	$d_{4 \rightarrow 8}$	$d_{4 \rightarrow 9}$	$d_{8 \rightarrow 10}$	$d_{9 \rightarrow 10}$
1.00	$0.274\hat{x}$	$0.382\hat{z}$	$0.279\hat{x}$	$0.731\hat{z}$	$0.210\hat{x}$	$0.281\hat{x}$	$0.058\hat{x}$	$0.853\hat{z}$	$0.832\hat{z}$	$0.349\hat{x}$
1.05	$0.265\hat{x}$	$0.417\hat{z}$	$0.269\hat{x}$	$0.704\hat{z}$	$0.192\hat{x}$	$0.272\hat{x}$	$0.114\hat{x}$	$0.841\hat{z}$	$0.629\hat{z}$	$0.329\hat{x}$
1.10	$0.250\hat{x}$	$0.440\hat{z}$	$0.255\hat{x}$	$0.661\hat{z}$	$0.166\hat{x}$	$0.260\hat{x}$	$0.153\hat{x}$	$0.814\hat{z}$	$0.456\hat{z}$	$0.300\hat{x}$
1.15	$0.235\hat{x}$	$0.447\hat{z}$	$0.243\hat{x}$	$0.620\hat{z}$	$0.144\hat{x}$	$0.250\hat{x}$	$0.170\hat{x}$	$0.787\hat{z}$	$0.356\hat{z}$	$0.270\hat{x}$
1.20	$0.215\hat{x}$	$0.446\hat{z}$	$0.229\hat{x}$	$0.564\hat{z}$	$0.113\hat{x}$	$0.237\hat{x}$	$0.183\hat{x}$	$0.530\hat{z}$	$0.263\hat{z}$	$0.223\hat{x}$

states 1–4 are larger than those of other doubly charged states when the laser couplings between N_2^{2+} states are ignored. However, these metastable states do not contribute the dissociation process of N_2^{2+} due to their long lifetime. Once the laser couplings between N_2^{2+} states are included, metastable states can be excited to dissociation states and thus contribute to subsequent dissociation. In the bottom panel of Fig. 3, we observe a significant decrease in the populations of metastable states 1–4, accompanied by a notable increase in the populations of dissociative states 5–10 when considering laser couplings between N_2^{2+} states. Specifically, the populations at the end of the laser pulse for states 1–4 decrease by 41.1%, 54.6%, 51.2%, and 66.2%, while states 5–10 increase by factors of approximately 16.1, 2.1, 2.8, 1.5, 3.3, and 22.7.

B. Nuclear vibrational effects on the SDI of N_2

To consider vibrational distributions of the ground state $X^1\Sigma_g^+$ of the neutral N_2 molecule, we numerically solve the time-independent Schrödinger equation for nuclear vibration

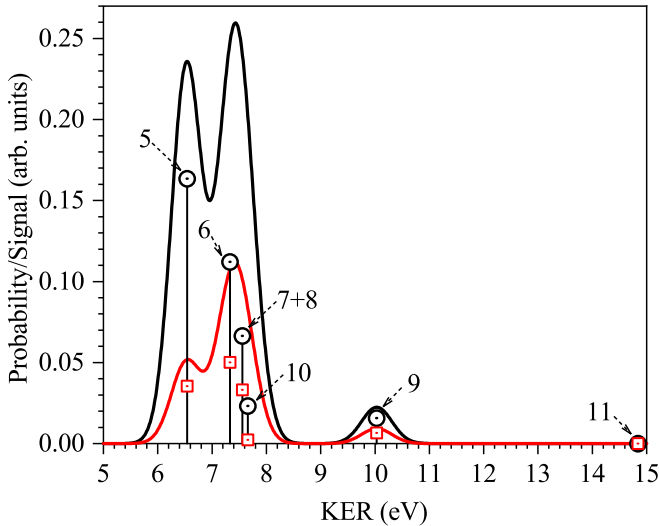


FIG. 2. Comparison of simulated KER spectra with (black line) and without (red line) laser couplings between N_2^{2+} states for N_2 frozen at the equilibrium internuclear distance. Alignment-averaged yield for dissociative N_2^{2+} states, obtained with and without the laser couplings between different N_2^{2+} states, are shown as circle and square symbols, respectively. We used a laser pulse with a peak intensity of 1.2×10^{15} W/cm², 8 fs FWHM, and a wavelength of 800 nm. The energy resolution is set to 0.28 eV.

motion of N_2 using the Fourier grid Hamiltonian method [39],

$$-\frac{\hbar^2}{2\mu} \frac{d^2 \varphi_k(R)}{dR^2} + V(R) \varphi_k(R) = E_k \varphi_k(R), \quad (8)$$

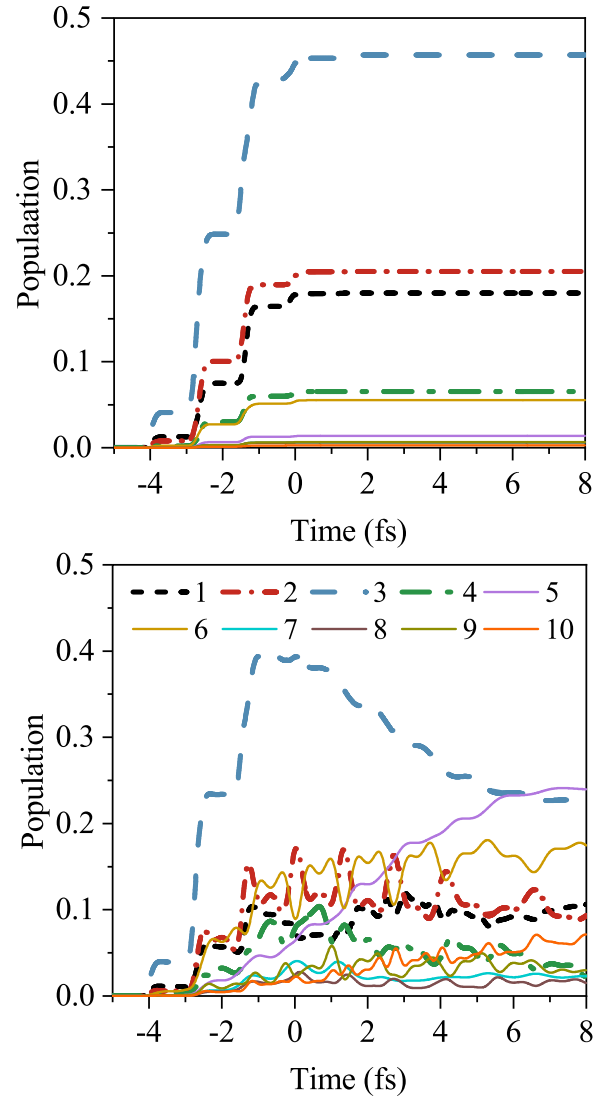


FIG. 3. Populations of N_2^{2+} states as function of time at $R = 1.10$ Å, with the laser polarization at 45° from the molecular axis. Top (bottom) shows the population without (with) laser couplings between N_2^{2+} states. In both cases, lines of the same color represent the same N_2^{2+} state, and the solid lines represent the dissociative states.

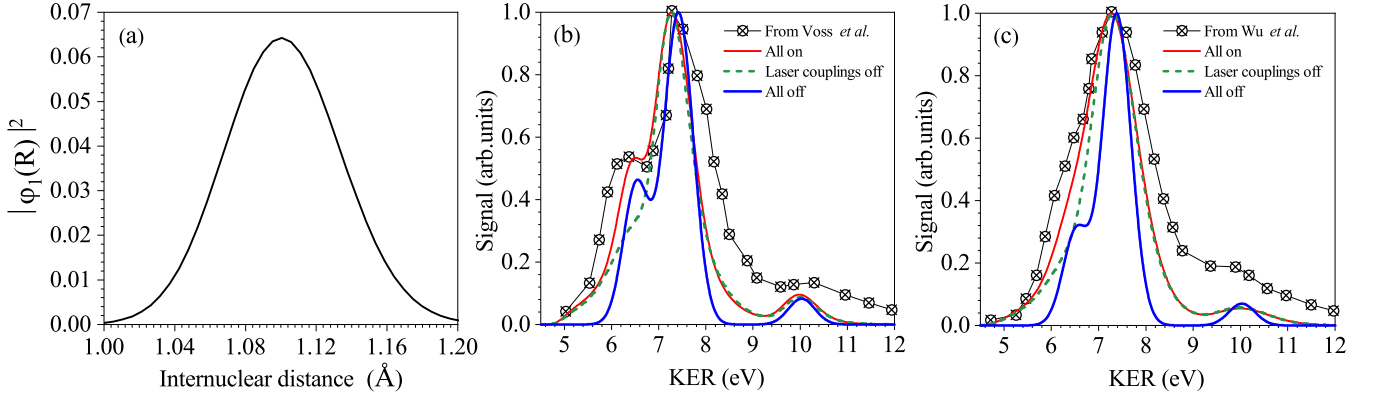


FIG. 4. (a) The probability density of the ground vibrational state of $X^1\Sigma_g^+$ of the neutral N_2 . (b) and (c) Comparison of the simulated KER spectra and the experimental data by (b) Voss *et al.* [3] with a peak intensity of 1.2×10^{15} W/cm², 8 fs FWHM, and a wavelength of 800 nm and by (c) Wu *et al.* [4] with a peak intensity of 7.5×10^{14} W/cm², 8 fs FWHM, and a wavelength of 780 nm. All on/off (red/blue solid lines): Both the nuclear vibrational motion and the laser couplings between the N_2^{2+} states are switched on/off. Green dashed lines: The nuclear vibrational motion is considered but the laser couplings between the N_2^{2+} states are switched off. The energy resolution σ is taken as $0.03 \times \text{KER}$ and $0.05 \times \text{KER}$ to reproduce the experimental results by Voss *et al.* [3] and Wu *et al.* [4], respectively.

where μ is the reduced mass, $V(R)$ is a modified Morse potential energy [40], R is the internuclear distance, and E_k is the vibrational energy. The probability density of the ground vibrational state of $X^1\Sigma_g^+$ is presented in Fig. 4(a). We see that it is sufficient to consider R from 1.0 to 1.2 Å.

By solving Eq. (1) at each internuclear distance, we obtain the probability of forming different N_2^{2+} states at different alignment angles θ . The alignment-averaged probability for the n th N_2^{2+} state at different internuclear distances is

$$\bar{P}_n(R) = \frac{1}{2} \int_0^\pi P_n(\theta, R) \sin \theta d\theta. \quad (9)$$

Then, similar to Eq. (7), the intensity of the KER spectra contributed from each R is

$$S(E, R) = \sum_n \frac{\bar{P}_n(R)}{\sqrt{2\pi\sigma^2}} \exp\left[-\frac{[E - E_n(R)]^2}{2\sigma^2}\right], \quad (10)$$

where $E_n(R)$ represents the KER values of state n at different R . Finally, convolving $S(E, R)$ with the probability density $|\varphi_1(R)|^2$, we obtain the averaged KER spectra as

$$\langle S(E) \rangle = \int_{1.0\text{\AA}}^{1.2\text{\AA}} S(E, R) |\varphi_1(R)|^2 dR. \quad (11)$$

To see the influence of the vibrational motion of N_2 on the KER spectra, we compare our theoretical calculations with the experimental results from Voss *et al.* [3] and Wu *et al.* [4] in Figs. 4(b) and 4(c). Note that we shifted the spectrum of Voss *et al.* [3] by -0.20 eV and that of Wu *et al.* [4] by 0.37 eV to match the position of the 7.43 eV KER peak.

As seen in Figs. 4(b) and 4(c), the KER spectra obtained from the improved DM-SDI model which includes the nuclear vibrational motion and the laser couplings between the N_2^{2+} states show better agreement with the experimental spectra, as compared to the results without accounting for the laser couplings or the nuclear vibrational motion. Particularly, using the improved DM-SDI model, the onset of the KER spectra is shifted from 6 to 5 eV, matching both experimental KER spectra. The ratio of the 6.54 eV to the 7.43 eV KER peak

values from the improved model also agrees better with the experiments. We should mention that the populations of the state 5 vary with the internuclear distance and thus the KER spectra sensitively depend on the internuclear distance (not shown). After convolving with the vibrational distribution of the ground state, the ratio of the 6.54 eV to the 7.43 eV KER peaks is significantly reduced by comparing the red line in Fig. 4(b) with the black line in Fig. 2. However, although the three KER peaks at 6.54, 7.43, and 10.03 eV are noticeably broader in the improved model, the width of the peaks are still narrower comparing to the experiments. This suggests that additional nuclear dynamics could be responsible for the spectral broadening, such as the velocity distribution of the initial nuclear wave packet as well as nuclear motion during the ionization process.

IV. SUMMARY AND OUTLOOK

To summarize, we improved the DM-SDI model developed by Yuen and Lin [23] by considering both the vibrational motion of the ground state of neutral N_2 and the laser couplings between N_2^{2+} states. The improved model can reproduce more features in the experimental KER spectra by Voss *et al.* [3] and Wu *et al.* [4], such as the onset of the spectra and the width of its peaks. Our results show that the laser couplings between N_2^{2+} states significantly enhance the yield of dissociative N_2^{2+} states, while nuclear vibration of the ground state of neutral N_2 contributes to part of the broadening of the spectra. This work provides a deeper understanding of dissociative sequential double ionization of molecules driven by strong laser IR fields. In the near future, we plan to investigate dissociative sequential triple or even quadruple ionization of molecules in superintense laser fields and propose some effective schemes for coherently controlling the total dissociation probabilities and their dissociation ratios.

ACKNOWLEDGMENTS

This work was supported by the National Natural Science Foundation of China (Grant No. 12164044). C.H.Y. and

C.D.L. were supported by Chemical Sciences, Geosciences and Biosciences Division, Office of Basic Energy Sciences,

Office of Science, U.S. Department of Energy under Grant No. DE-FG02-86ER13491.

- [1] C. Guo, M. Li, J. P. Nibarger, and G. N. Gibson, *Phys. Rev. A* **58**, R4271(R) (1998).
- [2] Y. H. Jiang, A. Rudenko, J. F. Pérez-Torres, O. Herrwerth, L. Foucar, M. Kurka, K. U. Kühnel, M. Toppin, E. Plésiat, F. Morales, F. Martín, M. Lezius, M. F. Kling, T. Jahnke, R. Dörner, J. L. Sanz-Vicario, J. van Tilborg, A. Belkacem, M. Schulz, K. Ueda *et al.*, *Phys. Rev. A* **81**, 051402 (2010).
- [3] S. Voss, A. S. Alnaser, X. M. Tong, C. Maharjan, P. Ranitovic, B. Ulrich, B. Shan, Z. Chang, C. D. Lin, and C. L. Cocke, *J. Phys. B: At. Mol. Opt. Phys.* **37**, 4239 (2004).
- [4] Z. F. Wu, C. Y. Wu, X. R. Liu, Y. K. Deng, and Q. H. Gong, *J. Phys. Chem. A* **114**, 6751 (2010).
- [5] C. Y. Wu, Y. D. Yang, Z. F. Wu, B. Z. Chen, H. Dong, X. R. Liu, Y. K. Deng, H. Liu, Y. Q. Liu, and Q. H. Gong, *Phys. Chem. Chem. Phys.* **13**, 18398 (2011).
- [6] X. K. Li, J. Q. Yu, H. Y. Xu, X. T. Yu, Y. Z. Yang, Z. Z. Wang, P. Ma, C. C. Wang, F. M. Guo, Y. J. Yang, S. Z. Luo, and D. J. Ding, *Phys. Rev. A* **100**, 013415 (2019).
- [7] T. Severt, Z. L. Streeter, W. Iskandar, K. A. Larsen, A. Gatton, D. Trabert, B. Jochim, B. Griffin, E. G. Champenois, M. M. Brister, D. Reedy, D. Call, R. Strom, A. L. Landers, R. Dörner, J. B. Williams, D. S. Slaughter, R. R. Lucchese, T. Weber, C. W. McCurdy *et al.*, *Nat. Commun.* **13**, 5146 (2022).
- [8] S. Zhao, B. Jochim, P. Feizollah, J. Rajput, F. Ziaee, Kanaka Raju P., B. Kaderiya, K. Borne, Y. Malakar, B. Berry, J. Harrington, D. Rolles, A. Rudenko, K. D. Carnes, E. Wells, I. Ben-Itzhak, and T. Severt, *Phys. Rev. A* **99**, 053412 (2019).
- [9] C. Cheng, R. Forbes, A. J. Howard, M. Spanner, P. H. Bucksbaum, and T. Weinacht, *Phys. Rev. A* **102**, 052813 (2020).
- [10] C. Cheng, Z. L. Streeter, A. J. Howard, M. Spanner, R. R. Lucchese, C. W. McCurdy, T. Weinacht, P. H. Bucksbaum, and R. Forbes, *Phys. Rev. A* **104**, 023108 (2021).
- [11] A. J. Howard, C. Cheng, R. Forbes, G. A. McCracken, W. H. Mills, V. Makhija, M. Spanner, T. Weinacht, and P. H. Bucksbaum, *Phys. Rev. A* **103**, 043120 (2021).
- [12] T. Severt, D. R. Daugaard, T. Townsend, F. Ziaee, K. Borne, S. Bhattacharyya, K. D. Carnes, D. Rolles, A. Rudenko, E. Wells, and I. Ben-Itzhak, *Phys. Rev. A* **105**, 053112 (2022).
- [13] S. Bhattacharyya, K. Borne, F. Ziaee, S. Pathak, E. Wang, A. S. Venkatachalam, N. Marshall, K. D. Carnes, C. W. Fehrenbach, T. Severt, I. Ben-Itzhak, A. Rudenko, and D. Rolles, *Phys. Chem. Chem. Phys.* **24**, 27631 (2022).
- [14] A. J. Howard, M. Britton, Z. L. Streeter, C. Cheng, R. Forbes, J. L. Reynolds, F. Allum, G. A. McCracken, I. Gabalski, R. R. Lucchese, C. W. McCurdy, T. Weinacht, and P. H. Bucksbaum, *Commun. Chem.* **6**, 81 (2023).
- [15] J. Ullrich, R. Moshhammer, R. Dörner, O. Jagutzki, V. Mergel, H. Schmidt-Böcking, and L. Spielberger, *J. Phys. B: At. Mol. Opt. Phys.* **30**, 2917 (1997).
- [16] J. Ullrich, R. Moshhammer, A. Dorn, R. Dörner, L. P. H. Schmidt, and H. Schmidt-Böcking, *Rep. Prog. Phys.* **66**, 1463 (2003).
- [17] A. T. Eppink and D. H. Parker, *Rev. Sci. Instrum.* **68**, 3477 (1997).
- [18] S. Saugout, E. Charron, and C. Cornaggia, *Phys. Rev. A* **77**, 023404 (2008).
- [19] X. H. Xie, K. Doblhoff-Dier, H. L. Xu, S. Roither, M. S. Schöffler, D. Kartashov, S. Erattupuzha, T. Rathje, G. G. Paulus, K. Yamanouchi, A. Baltuška, S. Gräfe, and M. Kitzler, *Phys. Rev. Lett.* **112**, 163003 (2014).
- [20] M. K. Lee, W. Li, and H. B. Schlegel, *J. Chem. Phys.* **152**, 064106 (2020).
- [21] P. Hoerner, W. Li, and H. B. Schlegel, *J. Chem. Phys.* **155**, 114103 (2021).
- [22] H. A. Leth, L. B. Madsen, and K. Mølmer, *Phys. Rev. Lett.* **103**, 183601 (2009).
- [23] C. H. Yuen and C. D. Lin, *Phys. Rev. A* **106**, 023120 (2022).
- [24] C. H. Yuen, P. Modak, Y. Song, S. F. Zhao, and C. D. Lin, *Phys. Rev. A* **107**, 013112 (2023).
- [25] C. H. Yuen and C. D. Lin, *Phys. Rev. A* **108**, 023123 (2023).
- [26] C. H. Yuen and C. D. Lin, *Phys. Rev. A* **109**, 033108 (2024).
- [27] C. H. Yuen and C. D. Lin, *Phys. Rev. A* **109**, L011101 (2024).
- [28] C. H. Yuen and C. D. Lin, *Commun. Phys.* **7**, 115 (2024).
- [29] D. Bhattacharya, K. R. Shamasundar, and A. Emmanouilidou, *J. Phys. Chem. A* **125**, 7778 (2021).
- [30] X. M. Tong, Z. X. Zhao, and C. D. Lin, *Phys. Rev. A* **66**, 033402 (2002).
- [31] S. F. Zhao, J. L. Xu, C. Jin, A.-T. Le, and C. D. Lin, *J. Phys. B: At. Mol. Opt. Phys.* **44**, 035601 (2011).
- [32] A. Pandey, B. Bapat, and K. R. Shamasundar, *J. Chem. Phys.* **140**, 034319 (2014).
- [33] H. Iwayama, T. Kaneyasu, Y. Hikosaka, and E. Shigemasa, *J. Chem. Phys.* **145**, 034305 (2016).
- [34] S. F. Zhao, C. Jin, A.-T. Le, T. F. Jiang, and C. D. Lin, *Phys. Rev. A* **81**, 033423 (2010).
- [35] S. F. Zhao, J. K. Li, G. L. Wang, P. C. Li, and X. X. Zhou, *Commun. Theor. Phys.* **67**, 289 (2017).
- [36] S. R. Langhoff, C. W. Bauschlicher, Jr., and H. Partridge, *J. Chem. Phys.* **87**, 4716 (1987).
- [37] S. R. Langhoff and C. W. Bauschlicher, Jr., *J. Chem. Phys.* **88**, 329 (1988).
- [38] I. Fdez. Galván, M. Vacher, A. Alavi, C. Angeli, F. Aquilante, J. Autschbach, J. J. Bao, S. I. Bokarev, N. A. Bogdanov, R. K. Carlson *et al.*, *J. Chem. Theory Comput.* **15**, 5925 (2019).
- [39] C. C. Marston and G. G. Balint-Kurti, *J. Chem. Phys.* **91**, 3571 (1989).
- [40] A. M. Desai, N. Mesquita, and V. Fernandes, *Phys. Scr.* **95**, 085401 (2020).